COMMUNICATION

Networking Pyrolyzed Zeolitic Imidazolate Frameworks by Carbon Nanotubes Improves Conductivity and Enhances Oxygen-Reduction Performance in Polymer-Electrolyte-Membrane Fuel Cells

Chao Zhang, Yu-Cheng Wang, Bing An, Ruiyun Huang, Cheng Wang, Zhiyou Zhou,* and Wenbin Lin**

With high thermodynamic energy conversion efficiency, proton-exchange-membrane fuel cells (PEMFC) have the potential to revolutionize green power.[1–3] However, PEMFCs cannot be used in large scale without the development of efficient nonprecious-metal catalysts (NPMCs) for the cathodic oxygen-reduction reaction (ORR).[4] Various transition-metal–nitrogen–carbons (TM-N-C, TM = Mn, Fe, Co, Ni, etc.) prepared from the pyrolysis of metal–organic hybrid precursors have shown promising ORR activity.[5–13] Zeolitic imidazolate frameworks (ZIFs), tetrahedrally coordinated transition-metal ions connected by imidazolate linkers, can serve as precursors for the pyrolysis.[14] Several highly active ORR catalysts have been developed from ZIFs[9,15–19] through judicious control of crystal morphology,[20] element doping,[21–24] and pyrolysis.[25] However, the majority of studies have focused on the performance of these catalysts in half cell reactions in aqueous media by linear scanning voltammetry (LSV). Complete liquid-free PEMFCs using pyrolyzed ZIFs as ORR catalysts have only been reported in a few cases.[14,17,18,26] Dodelet and co-workers used ZIF-8 (Zn) combined with additional iron complexes as precursors for high-performance cathode catalysts for the ORR in PEMFC, with a resultant PEMFC power density of 750 mW cm^{-2} at 0.6 V.[17] Meanwhile, Liu and co-workers systematically investigated combinations of different ZIFs and additional iron/cobalt sources as the pyrolysis precursor, revealing that the Fe source together with Zn-ZIF give a uniform distribution of Fe in the final N-doped carbon matrix and the best NPMCs.[18,26] Further development and understanding of not only the intrinsic activity of such catalysts but also the relevant conductivity and mass transport in the catalyst layer in full PEMFCs are highly desirable.[27]

In this work, we prepared a Fe-N-C catalyst by the pyrolysis of Fe-doped Zn-ZIF-8. Our direct doping of Fe^{3+} into the ZIF lattice differs from previous strategies which introduce Fe and Zn from different sources and may lead to more uniform inclusion of FeN_x centers into the resultant carbon matrix. The obtained catalyst after optimization gave an ORR half-wave potential of 0.81 V versus reversible hydrogen electrode (RHE) and a mass activity (j_m) of 17.22 A g^{-1} at 0.8 V in acidic media, an activity comparable to the highest of all reported NPMCs.[19] Such superior performance partially results from the vaporization of Zn at pyrolysis temperature, leaving a highly porous carbon matrix with uniformly distributed FeN_x active sites. We used this catalyst to construct a working PEMFC that exhibited a power density of 620 mW cm^{-2}, a value limited by the electronic conductivity of the Fe-C-N as indicated by the ohmic voltage loss on the polarization curve. To improve interparticle conductivity of the Fe-C-N catalysts, multiwalled carbon nanotubes (MWCTs) were introduced into the ZIF synthesis to interconnect the nanoparticles and provide electron-conducting highways (**Scheme 1**). Since addition of furfuryl alcohol (FA) as a second precursor in the pyrolysis has been shown to increase the surface area and carbon content of pyrolyzed ZIFs with enhanced ORR performance,[28,29] FA was added into the ZIF pores to further improve the intraparticle connectivity/conductivity and intrinsic ORR activity. After the improvement in connectivity, the power density of the PEMFC reached 820 mW cm^{-2}, a value comparable to that of the best NPMCs.[16,17]

The Fe-Zn bimetallic ZIFs (**ZIF′**) were prepared by mixing methanolic solutions of $Zn(NO_3)_2$ and $FeSO_4$ (molar ratio of Zn/Fe = 5–100) with 2-methylimidazole (2-mIm), followed by stirring for 24 h at room temperature. The multiwalled-carbon-nanotube (MWCNT)-templated samples (**ZIF′-CNT**) were prepared by adding MWCNT that had been surface functionalized with carboxylate groups in the reaction mixture. The actual molar ratios of Zn/Fe in the samples were determined by inductively coupled plasma atomic emission spectrometry analysis (Table S1, Supporting Information). Both **ZIF′** and **ZIF′-CNT** exhibit the same crystalline structure as ZIF-8, as shown by powder X-ray diffraction (PXRD) patterns (Figure S1 and S2, Supporting Information). **ZIF′** formed polyhedral nanocrystals

Dr. C. Zhang, Y.-C. Wang, B. An, R. Huang, Prof. C. Wang, Prof. Z. Zhou, Prof. W. Lin
Collaborative Innovation Center of Chemistry for Energy Materials
State Key Laboratory of Physical Chemistry of Solid Surfaces
Department of Chemistry
College of Chemistry and Chemical Engineering
Xiamen University
Xiamen 361005, P. R. China
E-mail: wangchengxmu@xmu.edu.cn; zhouzy@xmu.edu.cn; wenbinlin@uchicago.edu
Prof. W. Lin
Department of Chemistry
University of Chicago
929 E 57th Street, Chicago, IL 60637, USA

DOI: 10.1002/adma.201604556

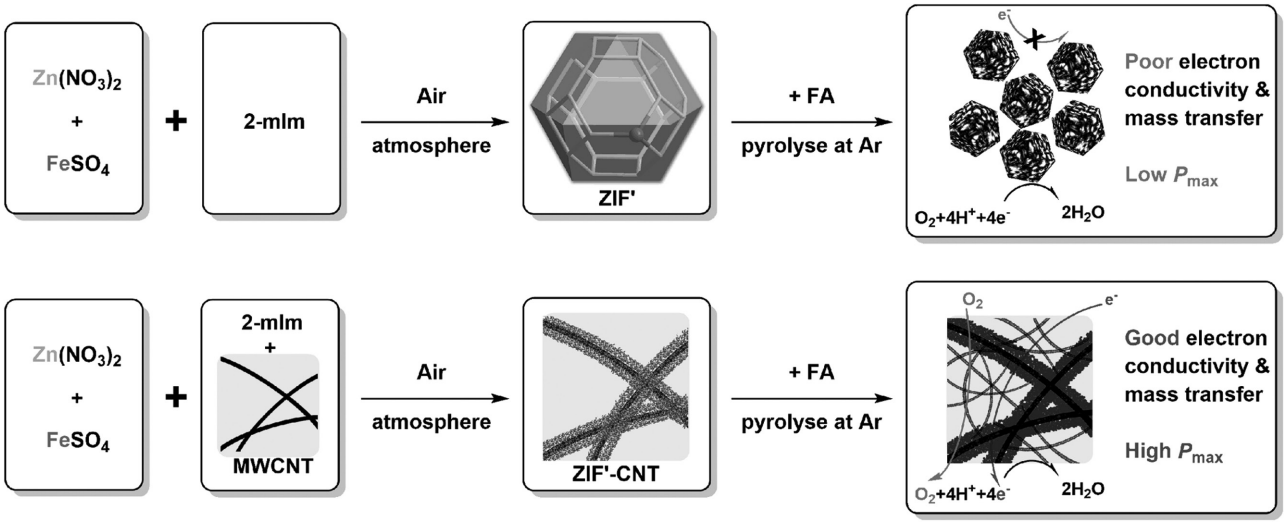

Scheme 1. To improve the interparticle conductivity of the Fe-C-N catalysts, multiwalled carbon nanotubes (MWCTs) were introduced into the ZIF synthesis to interconnect the nanoparticles and to provide electron-conducting highways.

with crystal diameters ranging from the sub-micrometer scale to 100 nm depending on the reaction condition (transmission electron microscopy = TEM, **Figure 1** and Figure S3, Supporting Information). In the MWCNT-templated **ZIF′-CNT**, **ZIF′** nanocrystals were strung into a network by the MWCNTs (Figure 1c and Figure S4, Supporting Information). The carboxylate functional groups on the MWCNT surface induced site-specific nucleation of ZIF crystals, yielding a CNT/ZIF hierarchical structure. **ZIF′** samples with various Zn/Fe ratios were pyrolyzed at 950 °C for 2 h. Partial aggregation of **ZIF′** particle was observed by TEM after the pyrolysis (Figure S3, Supporting Information), similar to what was observed for unprotected ZIF derived catalyst in literature.[30] Each of the pyrolyzed samples showed a weak and broad peak at $2\theta = 25°$ in PXRD, which corresponds to a partially graphitized carbon (**Figure 2** and Figure S5, Supporting Information).[19] The Fe was of 1–5 wt% of the pyrolyzed samples (**ZIF′-p**) and was distributed uniformly in the N-doped carbon matrix, as revealed by elemental mapping with energy dispersive X-ray (EDX) spectroscopy (Figure 1e). The oxidation state of the doped Fe was determined to be +3 based on X-ray photoelectron spectroscopy (Figure S6, Supporting Information).[31]

We also loaded FA to the inner pores of the **ZIF′** and the **ZIF′-CNT** to increase the surface area and carbon content of pyrolyzed ZIFs by soaking them in an FA solution overnight, then washing them with ethanol to remove the adsorbed FA on the external surface (denoted **ZIF′-FA** and **ZIF′-FA-CNT**). About 16 and 18 wt% of FA was loaded into the **ZIF′-FA** and **ZIF′-FA-CNT**, respectively, as estimated from thermogravimetric analysis (TGA) (Figure S7 and S8, Supporting Information). Neither the crystal structure nor the morphology of the ZIFs changed after the FA loading (Figure S9, Supporting Information). These FA-loaded ZIFs were first heated at 150 °C for 5 h to polymerize FA, then pyrolyzed at 950 °C for another 2 h, resulting in **ZIF′-FA-p** and **ZIF′-FA-CNT-p**. As expected, the samples loaded with FA showed much higher Brunauer–Emmett–Teller surface area (904.5 $m^2\ g^{-1}$ for **ZIF′-FA-p** vs 706.3 $m^2\ g^{-1}$ for **ZIF′-p**, Figure S10, Supporting Information). The **ZIF′-FA-CNT-p** showed less-defined Fe-N-C particles interconnected by MWCNTs on the TEM images (Figure 1d and Figure S11, Supporting Information). The weight percentage of MWCNT was 30–40% based on TGA and pyrolysis yield. There were also thinner CNTs growing out of the MWCNTs during the pyrolysis. This network of MWCNTs and the newly formed thin CNTs construct a conductive mesoporous framework to nest the active Fe-N-C ORR catalysts.

The ORR activities of these catalysts were evaluated in an O_2-saturated aqueous solution of 0.1 M $HClO_4$ using a rotating-disk electrode (RDE). The acid media were chosen to mimic the pH environment in a complete PEMFC. The electrode was prepared by drop casting a mixture of the pyrolyzed NPMCs with Nafion. The Zn/Fe ratios and pyrolysis conditions of **ZIF′-p** were optimized (**Figure 3**, and Figure S12 and S13, Supporting Information) to give an ORR onset potential of 0.95 V, a half-wave potential of 0.81 V versus RHE.[19] This activity was comparable to the best NPMCs. The number of electrons transferred (n) was 3.99 throughout the whole potential range, from 0.1 to 0.8 V, as calculated from the H_2O_2 percent yields (less than 1%) in the rotating ring disc electrode (Figure 3 and Figure S14, Supporting Information) measurements.

As anticipated, the addition of FA improved the ORR activity. For example, the **ZIF′-FA-p** exhibited half-wave potentials of ORR in the 0.80–0.82 V range, while those of **ZIF′-p** (molar ratio of Zn/Fe = 10–20) were only 0.76–0.79 V with lower mass activities (Figure S15, Supporting Information). We observed that the addition of MWCNT caused a slight decrease in specific ORR activity in aqueous solutions, due to increased catalyst mass from inactive MWCNT; however, further doping FA into **ZIF′-CNT-p** recovered a high level of ORR activity. As demonstrated in Figure S16 in the Supporting Information, the activity of **ZIF′-FA-CNT-p** (molar ratio of Zn/Fe = 20) was the highest of all the catalysts we built on a MWCNT template, with a half-wave potential of 0.80 V. To quantify the intrinsic activities that are free of mass transport limitations, kinetic currents were normalized with catalyst loadings to obtain mass activities (I_m) (see the Supporting Information). As demonstrated in

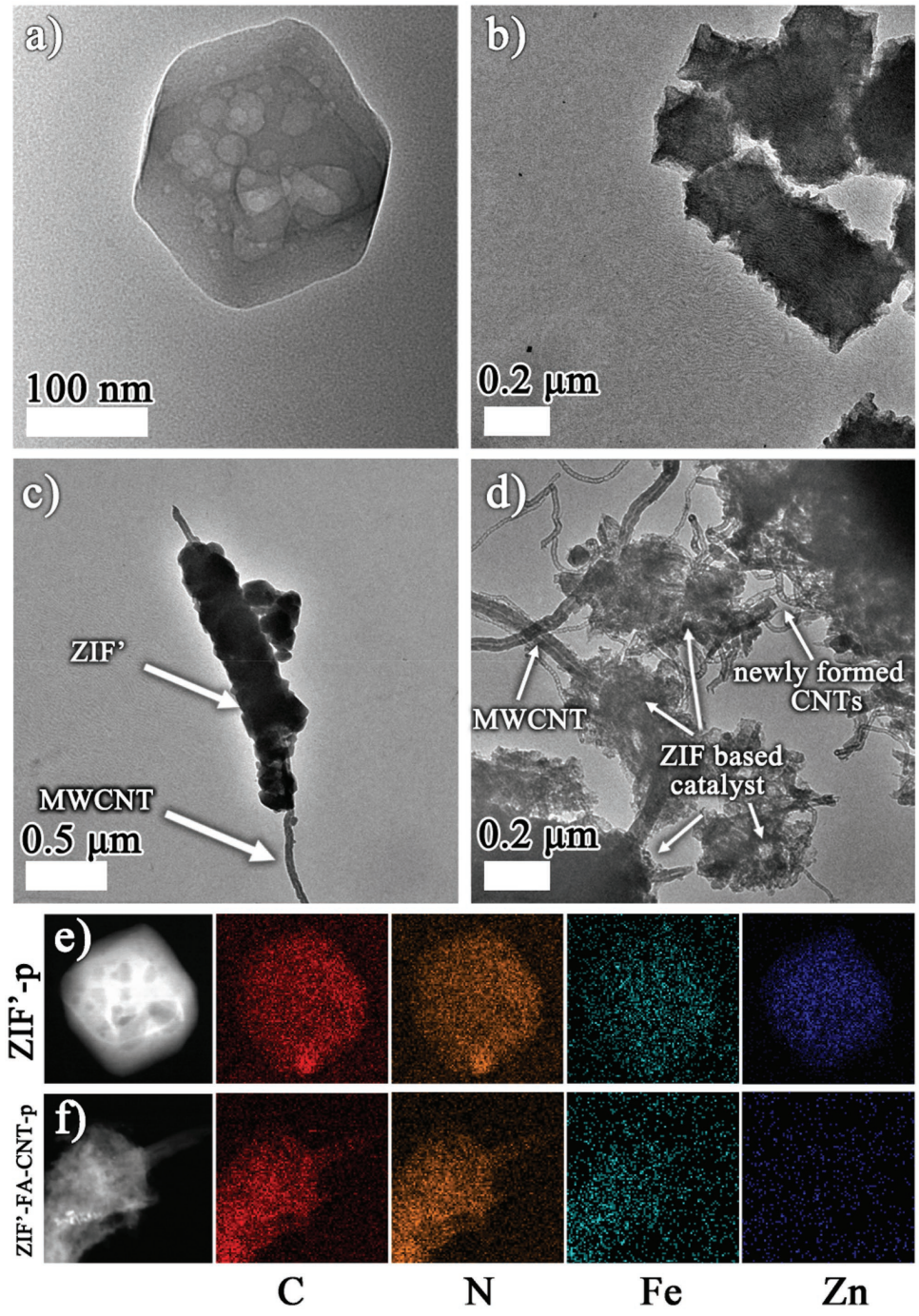

Figure 1. a–d) TEM images of **ZIF′** (a), **ZIF′-p** (b), **ZIF′-CNT** (c), and **ZIF′-FA-CNT-p** (d). e,f) EDX mapping of C, N, Fe, and Zn for **ZIF′-p** (e) and **ZIF′-FA-CNT-p** (f).

Figure S17 in the Supporting Information, the measured I_m at 0.80 V decreases in the order **ZIF′-FA-p** (18.43 A g^{-1}) > **ZIF′-p** (17.22 A g^{-1}) > **ZIF′-FA-CNT-p** (16.90 A g^{-1}) > **ZIF′-CNT-p** (11.65 A g^{-1}). A control experiment using pyrolyzed MWCNT without ZIF showed negligible ORR activity under the same conditions, verifying that the pyrolyzed ZIF was the active catalyst (Figure S18, Supporting Information). Furthermore, a simple mechanical mixture of MWCNT and NPMCs also showed a decrease in ORR activity in comparison to that derived from pre-assembled **ZIF′-FA-CNT** (Figure S19, Supporting Information).

We constructed PEMFCs from four optimized ORR catalysts: **ZIF′-p**, **ZIF′-FA-p**, **ZIF′-CNT-p**, and **ZIF′-FA-CNT-p** (**Figure 4**a). The PEMFC with **ZIF′-p** showed a maximum power density of 620 mW cm^{-2} at the cell potential of 0.34 V under optimized conditions, a value comparable to other reported ZIF-derived PEMFCs.[18]

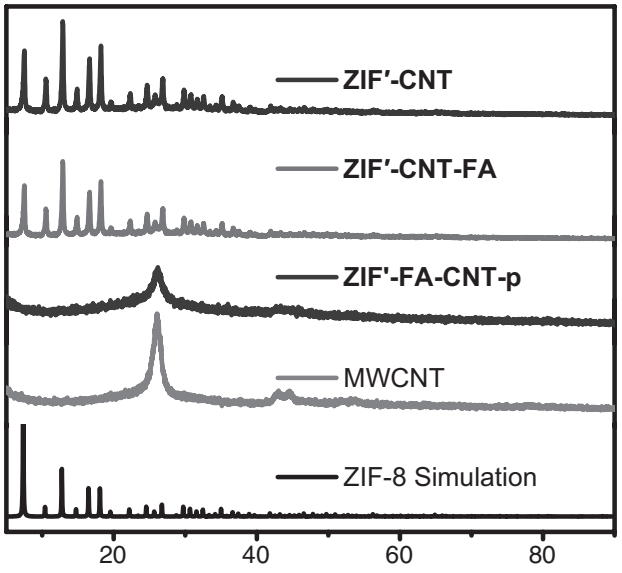

Figure 2. PXRD patterns of different samples.

The cell voltage (or power density) was limited by several factors in different regions of the polarization curves.[32] Typically, the region of low current density best represents the intrinsic catalytic activity of the catalyst. The voltage loss at an intermediate current density is caused by resistance to the flow of ions in the electrolyte and resistance to the flow of electrons through the electrode. At a high current density, the mass transport effect dominates, due to the limited transport of

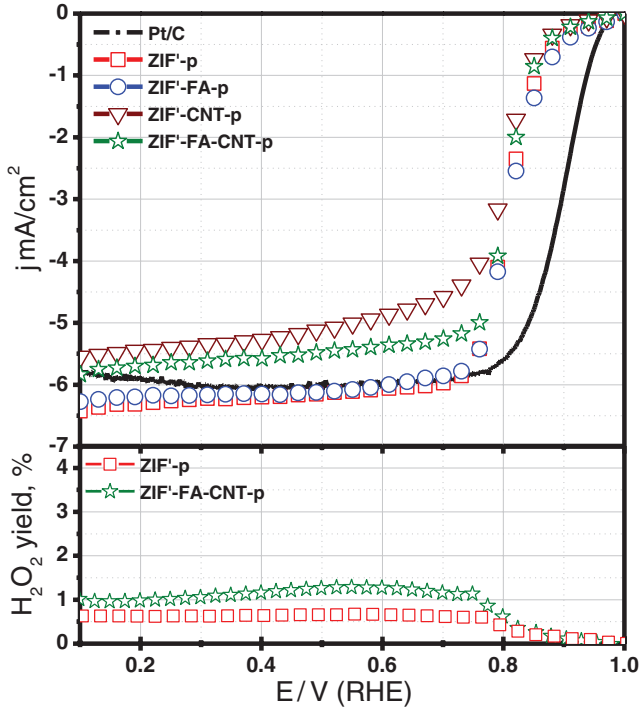

Figure 3. ORR polarization curves and H_2O_2 yield of different catalysts and Pt/C in O_2-saturated 0.1 M $HClO_4$ solution. Rotating speed: 1600 rpm; scan rate: 10 mV s^{-1}.

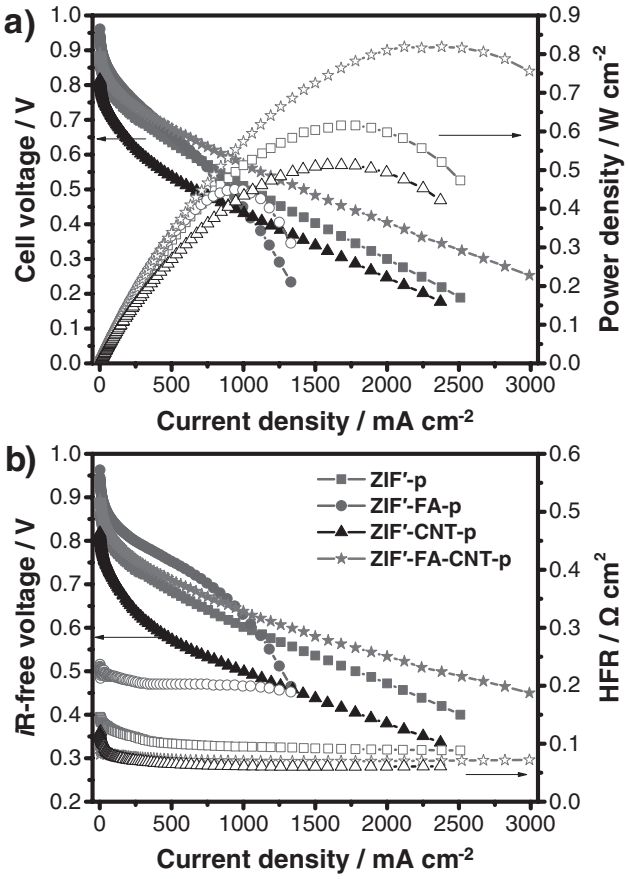

Figure 4. a) Polarization curves (left, filled symbols) and power density (right, open symbols) plots for H_2-O_2 PEMFC with **ZIF′-p**, **ZIF′-FA-p**, **ZIF′-CNT-p**, and **ZIF′-FA-CNT-p** as cathode catalysts at 80 °C; b) *i*R-free polarization curves (left, filled symbols) and high-frequency resistivities (right, open symbols) of **ZIF′-p**, **ZIF′-FA-p**, and **ZIF′-FA-CNT-p**. The back pressure was 1 bar as indicated; flow rate: 0.3 L min^{-1}; proton-exchange membrane: Nafion NRE 211 membrane.

oxygen and water vapor in catalyst layer.[33,34] The PEMFC with **ZIF′-p** as the ORR catalyst showed a relatively high cell voltage in the low current density region, indicating the high intrinsic activity of the catalyst. The addition of FA further increased the intrinsic activity of the ZIF derived catalysts, as shown by the low current density region of the polarization curve. Quantitatively, the *i*R-free current density at 0.8 V was used as an indicator to estimate the intrinsic ORR activities of the NPMCs.[21,25] The *i*R-free current density of **ZIF′-FA-p** at 0.8 V was 250 mA cm^{-2}, whereas the value of **ZIF′-p** was 60 mA cm^{-2} (Figure 4b). However, the addition of FA increases interparticle resistance and interrupts the mass transport through the particles. As a result, the polarization curve of **ZIF′-FA-p** dropped dramatically in the intermediate current density and high current density region.[9,16–18] Consistent with this, high-frequency resistivity increased from 0.09 Ω cm^2 of **ZIF′-p** to 0.21 Ω cm^2 of **ZIF′-FA-p**. HFR value is a measure of conductivity of ORR catalysts in PEMFC test. Because of this, the maximum power density of **ZIF′-FA-p** is only 440 mW cm^{-2} (Figure 4a). Another important parameter is the current density at 0.6 V, which is a reasonable voltage for practical operation. The current density

in this region was determined by both intrinsic catalytic activity and cell resistance, leading to 650 mA cm^{-2}@ 0.6 V for **ZIF′-FA-p**.

On the other hand, the MWCNT network significantly improved the conductivity of the system but reduced its intrinsic catalytic activity. Our MWCNT templating strategy decreased the HFR of the cell from ca. 0.21 Ω cm^2 (**ZIF′-FA-p**) to 0.058 Ω cm^2 (**ZIF′-CNT-p**, Figure 4b), resulting in a current density of 300 mA cm^{-2} @ 0.6 V and a maximum power density of 510 mW cm^{-2} @ 0.31 V for **ZIF′-CNT-p**, limited by the intrinsic catalytic activity of **ZIF′-CNT-p**. In comparison, the **ZIF′-FA-CNT-p** benefited from both FA doping, which boosted its intrinsic activity, and a mesoporous CNT network, which enhanced conductivity and mass transport. The measured HFR of **ZIF′-FA-CNT-p** in the PEMFC test was 0.08 Ω cm^2. Therefore, the current density at 0.6 V was 880 mA cm^{-2} and the maximum power density reached 820 mW cm^{-2}. These values are comparable to those of the best PEMFCs based on ORR NPMCs.

In order to compare the mass transport effects of different NPMCs, the polarization curves were fitted by a mathematical model considering electrode kinetics, *iR* drop, and diffusional resistance:[35–37]

$$V_{\text{cell}} = E_0 - b\log i - Ri + B\log\left(1 - \frac{i}{i_{\text{L}}^{\text{O}_2}}\right) \quad (1)$$

where V_{cell} is PEMFC working potential, i represents current density, E_0 is a parameter representing the open-circuit potential combined with terms from exchange current density, b is an apparent Tafel slope, R is an ohmic resistance, B is an empirical parameter. The factor $i^{\text{O}}{}_{2\text{L}}$represents the limiting current density due to a limited oxygen mass transport. As demonstrated in Figure S20 in the Supporting Information, this model gave good fittings between experimental polarization curves and simulated ones for NPMCs. The resultant $i^{\text{O}}{}_{2\text{L}}$ increased in the order of **ZIF′-FA-p** (1510 mA cm^{-2}) < **ZIF′-p** (3512 mA cm^{-2}) < **ZIF′-CNT-p** (3835 mA cm^{-2}) < **ZIF′-FA-CNT-p** (5531 mA cm^{-2}), indicating fast transport of oxygen in **ZIF′-FA-CNT-p** as compared to the other samples. Consistent with this observation, the pore-size distribution of **ZIF′-FA-CNT-p**, as derived from the gas adsorption measurement, showed a much higher percentage of mesopores in 10–50 nm range than that of **ZIF′-p** or **ZIF′-FA-p** (**Figure 5**). The Barrett–Joyner–Halenda (BJH) adsorption cumulative mesopore volumes increase in the order **ZIF′-FA-p** (0.24 cm^3 g^{-1}) < **ZIF′-p** (0.30 cm^3 g^{-1}) < **ZIF′-CNT-p** (0.32 cm^3 g^{-1}) < **ZIF′-FA-CNT-p** (0.42 cm^3 g^{-1}).

Although the optimized **ZIF′-p**, **ZIF′-FA-p**, **ZIF′-CNT-p**, and **ZIF′-FA-CNT-p** showed similar ORR activity (half-wave potentials differences <20 mV) in acidic aqueous solution measured on RDE (Figure 3), they performed differently in PEMFCs. In the solution phase measurement, protons can easily reach catalytic centers, and a sufficient oxygen supply is maintained by the rotation of the electrode. The current density in RDE LSV is thus generally determined by the intrinsic activity of the catalysts. In contrast, in the complete cell, protons can only be transported in the Nafion matrix, while electrons can only conduct through the carbon matrix of the ORR catalyst, and oxygen

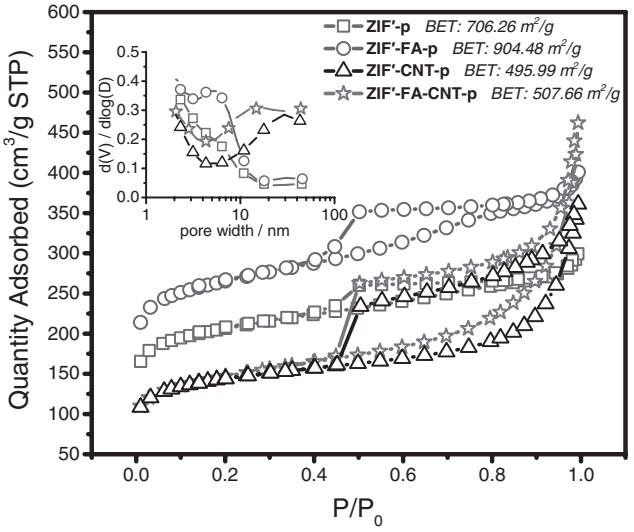

Figure 5. N_2 sorption isotherms of different samples and corresponding pore size distribution (BJH method).

is in the gas phase. The ORR can therefore only take place at the triple phase boundary. The formation of a bicontinuous heterostructure between the catalysts and the Nafion phase is thus of great value for the complete cell. Porosity is also required in between the two phases to allow for diffusion of oxygen and water vapor. As a result, the mesoporosity and the conductivity, especially the long-range interparticle conductivity of the catalysts, are key factors that dictate the ORR performance in PEMFC.

We further probed the chemical nature of the active sites of the catalysts by poisoning with thiocyanate (SCN^-). The drastic current drop in controlled potential electrolysis is consistent with FeN_x as the active sites (Figure S21, Supporting Information).[9,23] Like other NPMCs, **ZIF′-FA-CNT-p** is tolerant of methanol in contrast to Pt/C (Figure S22, Supporting Information), a property that is crucial for methanol fuel cells. The average H_2O_2 yield of **ZIF′-FA-CNT-p** is about 1.0% between 0.1 and 0.8 V (Figure S14, Supporting Information). The long-term durability of the PEMFC with **ZIF′-FA-CNT-p** as ORR catalyst was also tested by operating the cell at 0.50 V for 60 h. The current density of the cell decreased from 1.20 to 0.20 A cm^{-2} (Figure S23, Supporting Information). More work is still required to understand and improve this stability.

In summary, we have introduced MWCNTs to increase electronic conductivity and mass-transport of ORR catalysts derived from Zn-Fe bimetallic ZIFs. The MWCNTs interconnect the precursor ZIF crystals and form a network of electron highways after pyrolysis. The active Fe-N-C catalysts nest in the conducting web and utilize the electrons to reduce oxygen in the pores, leading to a current density of 880 mA cm^{-2} @ 0.6 V and a maximum power density of 820 mW cm^{-2} for the PEMFC. This work highlights the importance of hierarchical nanostructures of ORR catalysts for efficient electron, proton and mass transportation in PEMFC. We believe this templating strategy with conductive MWCNTs is a general method to construct designer nanoarchitectures in NPMCs for superior PEMFC performance.

Experimental Section

*Preparation of **ZIF′-CNT** Nanocrystals*: Typically, the mixture $Zn(NO_3)_2{\cdot}6H_2O$ and $FeSO_4{\cdot}7H_2O$ with a desired molar ratio of Zn^{2+}/Fe^{2+} was dissolved in 80 mL of methanol. A mixture of 2-methylimidazole (3.70 g) and MWCNT (0.1 g) with 80 mL methanol was added to the above solution with vigorous stirring for 24 h at room temperature. The total amount of (Zn + Fe) was fixed to be 5.65 mmol. The product was separated by centrifugation and washed thoroughly with ethanol for three times, and finally dried overnight at 50 °C.

*Preparation of **ZIF′-FA-CNT***: 0.3 g of **ZIF′-CNT** was dispersed in 5 mL FA. The mixture was vigorously stirred for 13 h at room temperature. The product was separated by centrifugation and washed thoroughly with ethanol once and finally dried overnight at 50 °C.

*Preparation of **ZIF′-FA-CNT-p***: 0.3 g of **ZIF′-FA-CNT-p** was transferred into a quartz boat and placed in a furnace under Ar flow (50–80 mL min^{-1}), and heated at 80 °C for 3 h and then at 150 °C for 5 h. Subsequently, carbonization of the composite was performed under Ar at 950 °C for 2 h with a heating rate of 5 °C min^{-1}, before being cooled to room temperature.

*Preparation of **PEMFC***: Under optimized condition, the membrane electrode assemblies (MEAs) consisted of **ZIF′-p** (4.5 mg cm^{-2}), **ZIF′-FA-p** (4.5 mg cm^{-2}), **ZIF′-CNT-p** (4.5 mg cm^{-2}) or **ZIF′-FA-CNT-p** (4.5 mg cm^{-2}) as cathode catalyst for ORR, and Pt/C (0.4 mg_{Pt} cm^{-2}) as anode catalyst for H_2 oxidation. PEMFC polarization and durability curves were obtained at 80 °C on Model 850e fuel cell test system (Scribner Associates Inc.). The flow rate was 0.2 standard liters per minute (slpm) for both anode (hydrogen) and cathode (oxygen) at 100% RH. NRE 211 membrane was applied in this work and the geometric surface area of the MEA was 1.69 cm^2. To enhance mass transfer, a back pressure of 1 bar was applied (absolute pressure of H_2 or O_2 was about 1.5 bar, respectively, considering 0.47 bar of water saturation vapor pressure at 80 °C). Considering the US Department of Energy (DOE) standard test for platinum-group-metals-free electrode catalyst (1 bar absolute O_2 pressure), the PEMFC areal current density can be corrected according to the following equation:[15,38,39]

$$I_M^* = I_M \left(P_{O_2}^* / P_{O_2}\right)^{0.79} \left(P_{H_2}^* / P_{H_2}\right)^{\alpha c/2} \quad (2)$$

where I_M is the mass activity obtained under absolute pressure P_{O_2} and P_{H_2} (1.5 bar); $P_{O_2}^*$ *and* $P_{H_2}^*$ are the absolute pressure of 1 bar. αc is the cathodic transfer coefficient.

Supporting Information

Supporting Information is available from the Wiley Online Library or from the author.

Acknowledgements

C. Z. and Y.-C.W. contributed equally to this work. The authors thank the Ministry of Science and Technology of P. R. China (2016YFA0200700), National Natural Science Foundation of P. R. China (21471126 and 21373175), US National Science Foundation (DMR-1308229), the National Thousand Talents Program of P. R. China, and the 985 Program of Chemistry and Chemical Engineering disciplines of Xiamen University for support with funding.

Received: August 25, 2016
Revised: October 1, 2016
Published online: November 22, 2016

[1] B. Dunn, H. Kamath, J.-M. Tarascon, *Science* **2011**, *334*, 928.
[2] J. B. Goodenough, *Acc. Chem. Res.* **2013**, *46*, 1053.
[3] P. G. Bruce, S. A. Freunberger, L. J. Hardwick, J.-M. Tarascon, *Nat. Mater.* **2012**, *11*, 172.
[4] R. Borup, J. Meyers, B. Pivovar, Y. S. Kim, R. Mukundan, N. Garland, D. Myers, M. Wilson, F. Garzon, D. Wood, P. Zelenay, K. More, K. Stroh, T. Zawodzinski, J. Boncella, J. E. McGrath, M. Inaba, K. Miyatake, M. Hori, K. Ota, Z. Ogumi, S. Miyata, A. Nishikata, Z. Siroma, Y. Uchimoto, K. Yasuda, K. Kimijima, N. Iwashita, *Chem. Rev.* **2007**, *107*, 3904.
[5] S. Yuan, J.-L. Shui, L. Grabstanowicz, C. Chen, S. Commet, B. Reprogle, T. Xu, L. Yu, D.-J. Liu, *Angew. Chem.* **2013**, *125*, 8507.
[6] G. Wu, K. L. More, C. M. Johnston, P. Zelenay, *Science* **2011**, *332*, 443.
[7] Z. Li, G. Li, L. Jiang, J. Li, G. Sun, C. Xia, F. Li, *Angew. Chem., Int. Ed.* **2015**, *54*, 1494.
[8] W. Niu, L. Li, X. Liu, N. Wang, J. Liu, W. Zhou, Z. Tang, S. Chen, *J. Am. Chem. Soc.* **2015**, *137*, 5555.
[9] Q. Wang, Z.-Y. Zhou, Y.-J. Lai, Y. You, J.-G. Liu, X.-L. Wu, E. Terefe, C. Chen, L. Song, M. Rauf, N. Tian, S.-G. Sun, *J. Am. Chem. Soc.* **2014**, *136*, 10882.
[10] M. Jahan, Q. Bao, K. P. Loh, *J. Am. Chem. Soc.* **2012**, *134*, 6707.
[11] H. T. Chung, J. H. Won, P. Zelenay, *Nat. Commun.* **2013**, *4*, 1922.
[12] Z. Zhuang, S. A. Giles, J. Zheng, G. R. Jenness, S. Caratzoulas, D. G. Vlachos, Y. Yan, *Nat. Commun.* **2016**, *7*, 10141.
[13] K. S. Park, Z. Ni, A. P. Côté, J. Y. Choi, R. Huang, F. J. Uribe-Romo, H. K. Chae, M. O'Keeffe, O. M. Yaghi, *Proc. Natl. Acad. Sci. USA* **2006**, *103*, 10186.
[14] S. Ma, G. A. Goenaga, A. V. Call, D.-J. Liu, *Chem.–Eur. J.* **2011**, *17*, 2063.
[15] M. Lefèvre, E. Proietti, F. Jaouen, J.-P. Dodelet, *Science* **2009**, *324*, 71.
[16] Y.-C. Wang, Y.-J. Lai, L. Song, Z.-Y. Zhou, J.-G. Liu, Q. Wang, X.-D. Yang, C. Chen, W. Shi, Y.-P. Zheng, M. Rauf, S.-G. Sun, *Angew. Chem., Int. Ed.* **2015**, *54*, 9907.
[17] E. Proietti, F. Jaouen, M. Lefèvre, N. Larouche, J. Tian, J. Herranz, J.-P. Dodelet, *Nat. Commun.* **2011**, *2*, 416.
[18] D. Zhao, J.-L. Shui, L. R. Grabstanowicz, C. Chen, S. M. Commet, T. Xu, J. Lu, D.-J. Liu, *Adv. Mater.* **2014**, *26*, 1093.
[19] X. Wang, H. Zhang, H. Lin, S. Gupta, C. Wang, Z. Tao, H. Fu, T. Wang, J. Zheng, G. Wu, X. Li, *Nano Energy* **2016**, *25*, 110.
[20] W. Xia, J. Zhu, W. Guo, L. An, D. Xia, R. Zou, *J. Mater. Chem. A* **2014**, *2*, 11606.
[21] B. You, N. Jiang, M. Sheng, W. S. Drisdell, J. Yano, Y. Sun, *ACS Catal.* **2015**, *5*, 7068.
[22] Y.-Z. Chen, C. Wang, Z.-Y. Wu, Y. Xiong, Q. Xu, S.-H. Yu, H.-L. Jiang, *Adv. Mater.* **2015**, *27*, 5010.
[23] C. Zhang, B. An, L. Yang, B. Wu, W. Shi, Y.-C. Wang, L.-S. Long, C. Wang, W. Lin, *J. Mater. Chem. A* **2016**, *4*, 4457.
[24] Y. Qian, J. Cavanaugh, I. A. Khan, X. Wang, Y. Peng, Z. Hu, Y. Wang, D. Zhao, *ChemPlusChem* **2016**, *81*, 718.
[25] X. Wang, J. Zhou, H. Fu, W. Li, X. Fan, G. Xin, J. Zheng, X. Li, *J. Mater. Chem. A* **2014**, *2*, 14064.
[26] D. Zhao, J.-L. Shui, C. Chen, X. Chen, B. M. Reprogle, D. Wang, D.-J. Liu, *Chem. Sci.* **2012**, *3*, 3200.
[27] J. Shui, C. Chen, L. Grabstanowicz, D. Zhao, D.-J. Liu, *Proc. Natl. Acad. Sci. USA* **2015**, *112*, 10629.
[28] H.-L. Jiang, B. Liu, Y.-Q. Lan, K. Kuratani, T. Akita, H. Shioyama, F. Zong, Q. Xu, *J. Am. Chem. Soc.* **2011**, *133*, 11854.
[29] A. Aijaz, N. Fujiwara, Q. Xu, *J. Am. Chem. Soc.* **2014**, *136*, 6790.
[30] L. Shang, H. Yu, X. Huang, T. Bian, R. Shi, Y. Zhao, G. I. N. Waterhouse, L.-Z. Wu, C.-H. Tung, T. Zhang, *Adv. Mater.* **2016**, *28*, 1668.
[31] C. D. Wagner, W. M. Riggs, L. E. Davis, J. F. Moulder, *Handbook of X-Ray Photoelectron Spectroscopy: A Reference Book of Standard Data for Use in X-Ray Photoelectron Spectroscopy*, (Ed: G. E. Muilenberg), Perkin-Elmer Corporation, Physical Electronics Division, Eden Prairie, MN, USA **1979**.
[32] X.-Z. Yuan, H. Wang, in *PEM Fuel Cell Electrocatalysts and Catalyst Layers: Fundamentals and Applications*, (Ed: J. Zhang), Springer, London, UK **2008**, pp. 1–87.

[33] J. H. Hirschenhofer, D. B. Stauffer, R. R. Engleman, *Fuel Cells: A Handbook (Revision 3)*, USDOE, Washington, DC, USA, **1994**.
[34] *PEM Fuel Cell Diagnostic Tools*, (Eds: H. Wang, X. -Z. Yuan, H. Li), CRC Press, Boca Raton, FL, USA, **2011**.
[35] D. R. Sena, E. A. Ticianelli, V. A. Paganin, E. R. Gonzalez, *J. Electroanal. Chem.* **1999**, *477*, 164.
[36] U. Beuscher, *J. Electrochem. Soc.* **2006**, *153*, A1788.
[37] *PEM Fuel Cell Diagnostic Tools*, (Eds: H. H. Wang, X.-Z. Yuan, H. Li), CRC Press, Boca Raton, FL, USA **2012**.
[38] K. C. Neyerlin, W. Gu, J. Jorne, H. A. Gasteiger, *J. Electrochem. Soc.* **2006**, *153*, A1955.
[39] F. Jaouen, V. Goellner, M. Lefèvre, J. Herranz, E. Proietti, J. P. Dodelet, *Electrochim. Acta* **2013**, *87*, 619.